Research Article Vol. 6, No. 3 / March 2019 / Optica 280

Towards intense isolated attosecond pulses from relativistic surface high harmonics

Olga Jahn,[1,2] Vyacheslav E. Leshchenko,[1,2,*] Paraskevas Tzallas,[3,4] Alexander Kessel,[1,2] Mathias Krüger,[1,2] Andreas Münzer,[1,2] Sergei A. Trushin,[1,2] George D. Tsakiris,[1] Subhendu Kahaly,[4] Dmitrii Kormin,[1,2] Laszlo Veisz,[1,5] Vladimir Pervak,[1,2] Ferenc Krausz,[1,2] Zsuzsanna Major,[1,2,6] and Stefan Karsch[1,2,7]

[1]Max-Planck-Institut für Quantenoptik, Hans-Kopfermann-Str. 1, 85748 Garching, Germany
[2]Department für Physik, Ludwig-Maximilians-Universität München, Am Coulombwall 1, 85748 Garching, Germany
[3]Foundation for Research and Technology-Hellas, Institute of Electronic Structure and Laser, Heraklion, Crete, Greece
[4]ELI-ALPS, ELI-HU Non-Profit Ltd., Dugonics tér 13, Szeged 6720, Hungary
[5]Department of Physics, Umeå University, Umeå, Sweden
[6]Current address: GSI Helmholtzzentrum für Schwerionenforschung GmbH, Planckstraße 1, 64291 Darmstadt, Germany & Helmholtz-Institut Jena, Fröbelstieg 3, 07743 Jena, Germany
[7]e-mail: stefan.karsch@mpq.mpg.de
*Corresponding author: vyacheslav.leshchenko@mpq.mpg.de

Received 15 October 2018; revised 21 January 2019; accepted 29 January 2019 (Doc. ID 347449); published 4 March 2019

Relativistic surface high harmonics have been considered a unique source for the generation of intense isolated attosecond pulses in the extreme ultra-violet and x-ray spectral ranges. Their practical realization, however, is still a challenging task and requires identification of optimum experimental conditions and parameters. Here, we present measurements and particle-in-cell simulations to determine the optimum values for the most important parameters. In particular, we investigate the dependence of harmonics efficiency, divergence, and beam quality on the pre-plasma scale length as well as identify the optimum conditions for generation of isolated attosecond pulses by measuring the dependence of the harmonics spectrum on the carrier–envelope phase of the driving infrared field.

https://doi.org/10.1364/OPTICA.6.000280

1. INTRODUCTION

The invention of sources of attosecond pulses based on high-order harmonic generation (HHG) [1–3] has opened the field of attosecond science [4,5] with a wide range of potential applications [6]. Nowadays, attosecond science is based mainly on the HHG in gas media, which allows the generation of isolated attosecond pulses on the nano- to few-microjoule energy level with photon energies up to sub-keV. Unfortunately, microjoule energies and high conversion efficiency of $\sim 10^{-4}$ are achievable only in the spectral range below 30 eV and were demonstrated [7,8] with Xe gas jets, whereas at higher photon energies, the efficiency quickly decreases and does not exceed 10^{-6} [9,10]. The main problem with the HHG in gases is fundamental limitations determined by the ionization threshold of the gas medium [4,11], leading to severe restrictions on the extreme ultra-violet (XUV) flux, especially at high photon energies.

A way to overcome this limitation is to use relativistic harmonics generated by interaction of intense few-cycle laser fields with solid surfaces [12–15]. Theoretical predictions, based on the relativistic oscillating mirror (ROM) model [13], have suggested that intense isolated attosecond pulses with up to few keV photon energy can be generated when using few-cycle near-infrared (NIR) laser pulses with an intensity of $\sim 10^{20}$ W/cm^2. Therefore, ROM harmonics present one of the most promising attosecond sources for pump–probe studies in the x-ray spectral range. Yet, experimental obstacles associated mainly with the stringent requirements on the temporal contrast of the driving laser pulses have not yet allowed sufficient progress to realize the potential of this approach. However, recent progress in the development of laser systems based on optical parametric chirped-pulse amplification (OPCPA) with pump pulse durations between 1 ps [16] and 80 ps [17] made the required pulse parameters available. Although the generation of isolated attosecond pulses from relativistic laser–plasma interactions driven by few-cycle optical pulses has been theoretically predicted using one-dimensional particle-in-cell (1D PIC) simulations [15,18], its experimental realization remains open.

Viable laboratory scale alternatives in the multi-keV and especially MeV spectral ranges are x-ray sources based on laser–plasma accelerators [19,20] (Fig. 1), but the pulse duration of such sources is limited to a few femtoseconds so far, and conversion efficiency does not exceed 10^{-7}. In the spectral range ~100 eV–20 keV, large scale x-ray free electron lasers (XFELs) [25–27,29]

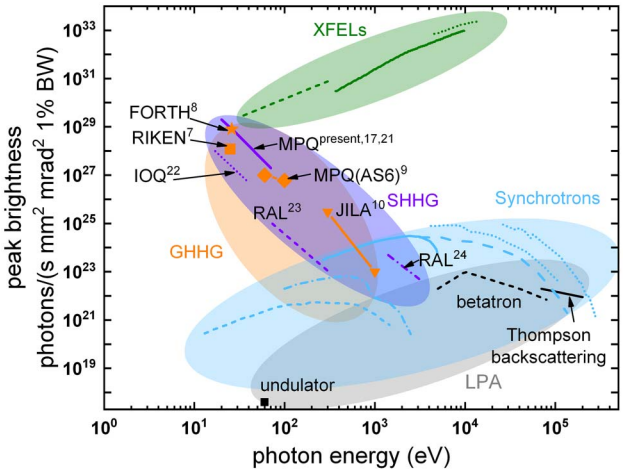

Fig. 1. Peak brightness for different types of x-ray sources: (violet area and lines) surface high-order harmonic generation (SHHG) [17, 21–24] and present work; (orange area, lines and points) gas-based high-order harmonic generation (GHHG) [7–10]; (gray area, black lines and points) sources based on laser-plasma accelerators (LPA) [19,20]; (green area and lines) XFELs (FLASH, LCLS, SACLA, etc.) [25–27]; (light blue area and lines) synchrotrons (BESSY, NSLS, PETRA, etc.) [26–28]. Shaded areas approximately mark the range of the demonstrated performance; lines and points mark examples and most important achievements. Note that out of the marked achievements, only results from MPQ [9,17,21], including present work and RIKEN [7], support isolated attosecond pulses.

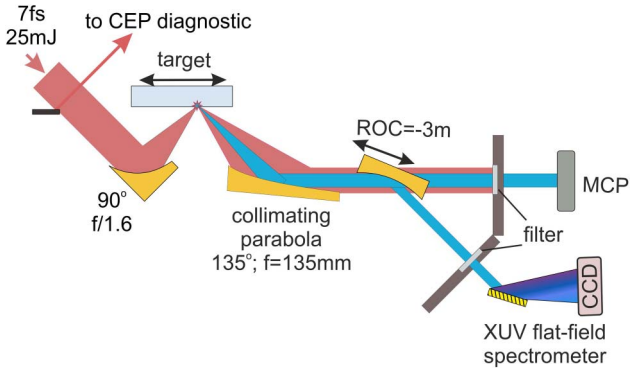

Fig. 2. Schematic setup of the experiment on the generation and characterization of relativistic surface high harmonics.

currently provide some unique parameters that are not accessible for laser-based sources yet, but they suffer from coherence problems, and the minimum achieved pulse duration is limited to a few femtoseconds [30]. Another problem with XFELs is the difficulty in sub-fs synchronization with laser sources, which can be useful for applications in atomic, molecular, and optical (AMO) physics.

Here, using a 10 Hz repetition rate laser system [16], delivering 7 fs pulses with 25 mJ energy at 900 nm central wavelength and better than 10^{-11} temporal contrast on the few-ps timescale, we experimentally investigate the dependence of the surface harmonics on the CEP of the driving field and demonstrate conditions under which isolated attosecond pulses can be generated. In addition, a direct measurement of the dependence of the harmonic efficiency, spectrum, beam profile, and divergence on the pre-plasma scale length is performed in order to determine the optimum conditions for generation of high-energy, high-quality XUV pulses. The experimental results are supported by PIC simulations.

2. EXPERIMENTAL SETUP

The experiment (Fig. 2) was performed by focusing p-polarized optical pulses onto a disk-like BK7 target under an incidence angle of 45° using a $f/1.6$ gold-coated 90° off-axis parabola. The peak intensity on target was 4×10^{19} W/cm^2 resulting in a normalized vector potential of $a_0 = 4.8$, where $a_0^2 = I\lambda^2/(1.37 \times 10^{18})$ with I being the laser intensity in W/cm^2 and λ the central wavelength in μm. The value of a_0, averaged over the full width at half maximum (FWHM) beam diameter, was around 3; therefore, $a_0 = 3$ was used in our 1D PIC simulations. As shown in previous experiments on relativistic surface HHG, it is the most efficient when the pre-plasma has a scale length approximately in the range $L_p \approx 0.1\lambda - 0.3\lambda$ [22,31,32]. To optimize the pre-plasma parameters, a pre-pulse with an intensity of about 10^{15} W/cm^2 and an adjustable delay (τ) was introduced before the main pulse [31] to pre-ionize the target and initiate the plasma expansion with the speed of $C_s \approx 80$ nm/ps [33], leading to an exponential [34] plasma density gradient at the solid–vacuum interface with the scale length of $L_p = C_s \times \tau$. The generated harmonics were collimated with a gold-coated off-axis parabola (50 × 50 mm clear aperture, 135 mm focal distance, 135° off-axis angle). A part of the recollimated beam was sent into a home-built XUV flat-field spectrometer consisting of a gold-coated grazing incidence grating (Hitachi 001-0266) and a XUV CCD camera (Andor DO440). A rectangular gold-coated spherical mirror (acting nearly as a cylindrical one under the incidence angle of 67.5°) with the radius of curvature of −3 m was used before the spectrometer in order to focus the beam in the non-diffraction dimension and to improve the signal-to-noise ratio of detected spectra. The mirror guiding the beam to the spectrometer was motorized to enable optimization of the incoupling and could be entirely moved out of the beam path to allow the measurement of the XUV beam profile with a micro-channel plate (MCP) detector and a phosphor screen (Photonis E3075-25-I60-PS20-FM8, 3 inch diameter). The residual NIR radiation was filtered out by a 650 nm thick aluminum foil placed in front of the MCP and a 200 nm thick aluminum or zirconium filter in front of the spectrometer. The maximum acquisition rate of the spectrometer XUV CCD camera limited the experimental repetition rate to 0.5 Hz. The CEP of the driving pulses was measured with a home-built single-shot $f-2f$ spectral interferometer (Fig. 2(b) in [35]). The CEP diagnostic provided only relative values; therefore, the absolute CEP was determined by fitting the experimental data to the simulations. In order to exclude the uncertainty introduced in the $f-2f$ measurements [36] by the energy instability of the driving pulses, their energy and the spectrum were recorded in parallel with the harmonic spectra and the $f-2f$ signal (for more detail, see Supplement 1). Note that all data were measured in a single-shot regime. The post-selection of the laser shots with energy instability <1% ensured the CEP uncertainty of less than ~200 mrad [36].

3. PLASMA SCALE LENGTH OPTIMIZATION

A typical measured spectrum of the generated harmonics is shown in Fig. 3. The harmonics exceed the coherent wake emission

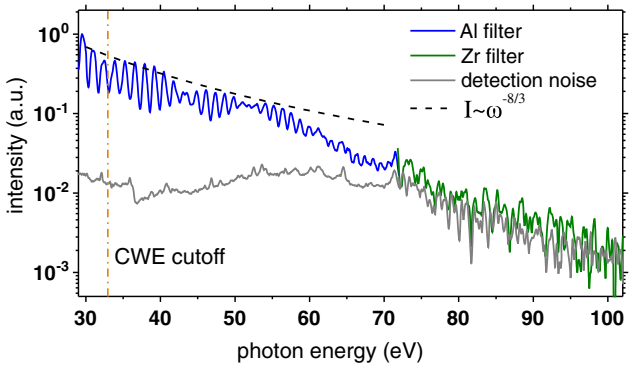

Fig. 3. Spectrum of the generated harmonics measured for $L_p \approx 0.2\lambda$ with aluminum (Al) and zirconium (Zr) filters with 200 nm thickness. The orange dashed-dotted line marks the CWE cutoff. The measured spectrum can be fitted with the power scaling law of $n \approx -2.8 \pm 0.3$ below 60 eV (see main text for more details), which is in a good agreement with the harmonics scaling predicted in BGP theory [14] represented by the black dashed line.

(CWE) [37] cutoff for a BK7 target of about 33 eV by a long way and reach photon energies above 70 eV, which infers the relativistic generation mechanism. The exponents in the harmonic power scaling law ($I \propto \omega^{-n}$) are $n \approx 2.8 \pm 0.3 \approx 8/3$ below 60 eV photon energy and $n \approx 5.5$ above 60 eV when fitting the envelope of the modulation structure. The scaling law below 60 eV agrees well with the value of $n \approx 8/3$ predicted by the Baeva–Gordienko–Pukhov (BGP) theory [14]. Also, the turning point at approximately 60 eV is in agreement with the theoretically expected cutoff [13] at ≈55 eV obtained for $a_0 = 3$. For the following investigations, we will limit ourselves to the spectral range transmitted by the Al filter (<70 eV), since this range provides the best signal-to-noise ratio (cf. Fig. 3).

One of the most important quality measures of high-harmonic generation is conversion efficiency. The XUV energy was estimated by using the collection efficiency and reflectivity/transmission of the optics, and the spectral response of the spectrometer. The experimentally measured harmonics conversion efficiency in dependence on the pre-plasma scale length is plotted in Fig. 4(a) showing a clear optimum at $L_p \approx 0.2\lambda$. This finding is in good agreement with the results of a 1D PIC simulation [38], as presented in Fig. 4(b). In particular, both experimental and numerical results have their maximum at about 0.2λ and exhibit a fast drop in

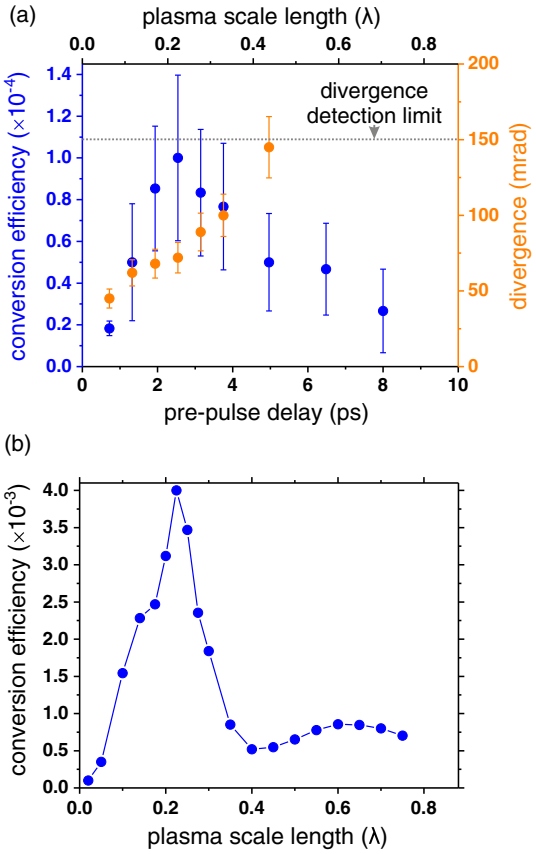

Fig. 4. (a) Experimental results on the harmonics conversion efficiency in the spectral range 30–70 eV (blue) and FWHM divergence of the XUV beam before collimation (orange). The maximum detectable divergence is limited by the aperture of the optical elements in the diagnostic beamline. (b) PIC simulations of the harmonics conversion efficiency in the spectral range 30–70 eV assuming $a_0 = 3$, $\tau = 2.5\lambda/c \sim 7$ fs. Each numerical data point is computed by averaging eight results with different carrier–envelope phases equally distributed between 0 and 2π.

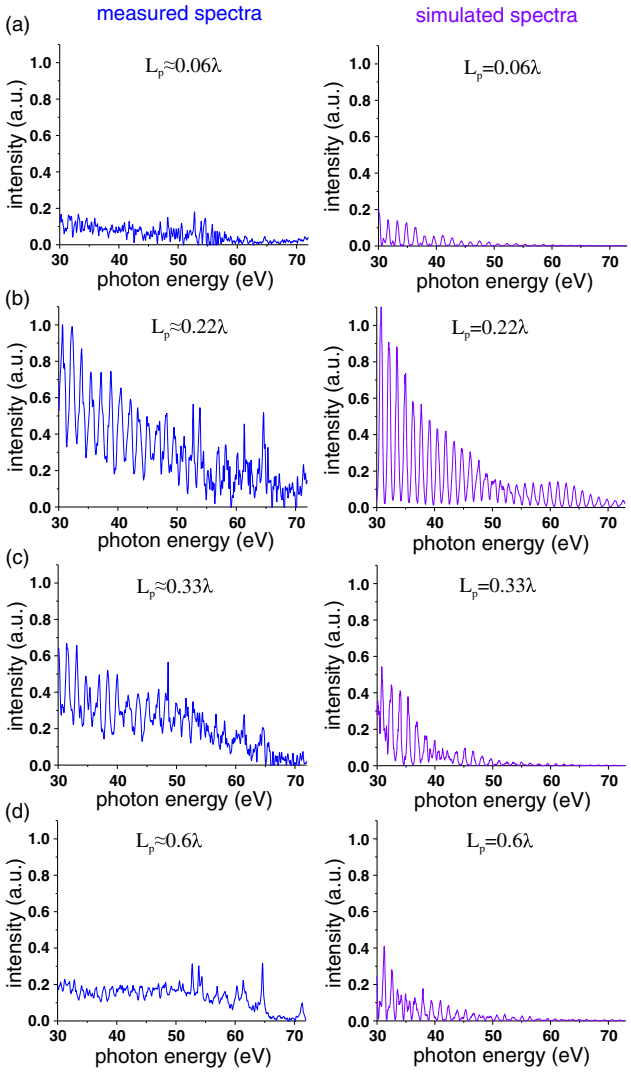

Fig. 5. Measured harmonic spectra (left panels) and corresponding simulated spectra (right panels) for $L_p \approx 0.06\lambda$ (a), $L_p \approx 0.22\lambda$ (b), $L_p \approx 0.33\lambda$ (c), and $L_p \approx 0.6\lambda$ (d).

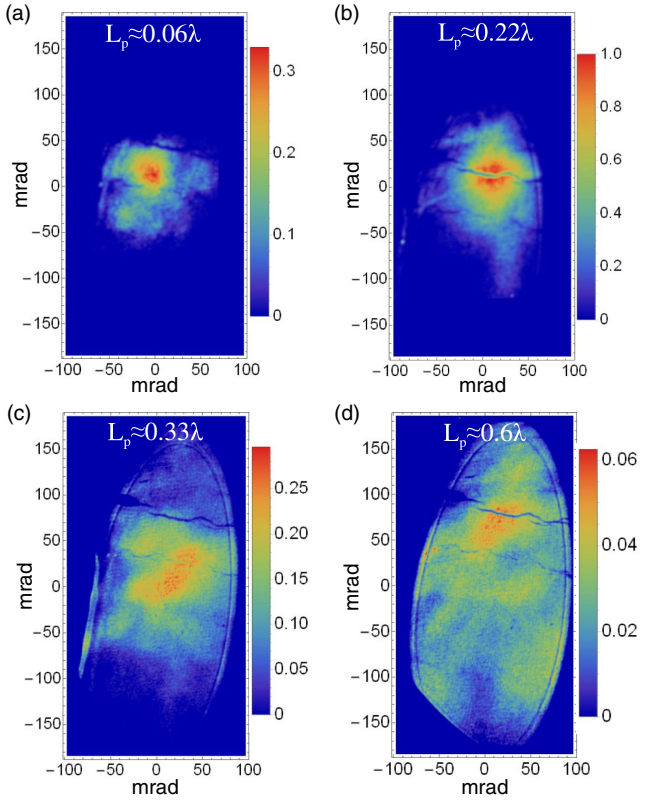

Fig. 6. Measured harmonics beam profile (single-shot data) for $L_p \approx 0.06\lambda$ (a), $L_p \approx 0.22\lambda$ (b), $L_p \approx 0.33\lambda$ (c), and $L_p \approx 0.6\lambda$ (d). The sharp edges are caused by hard clipping on the components in the diagnostic beamline.

efficiency for smaller and larger plasma scale lengths. This underlines the key importance of pre-plasma optimization for highest XUV conversion efficiencies. The maximum value of the efficiency in simulations is higher than in the experiment, but it is known that 1D PIC simulations provide approximately an order of magnitude higher efficiency compared to 2D PIC simulations for the same parameters [39]. Note that the measured conversion efficiency of $\eta \approx 10^{-4}$ at the optimum plasma conditions is significantly higher than the typical conversion efficiency of about 10^{-6} for gas harmonics in the comparable spectral range [9,40].

Another key quality measure for many applications is the focused XUV intensity, so the beam quality and divergence of the generated harmonics were measured simultaneously with the spectra (Fig. 5) and the energy. The XUV beam profiles were recorded after the collimating parabola for different plasma scale lengths and are presented in Fig. 6. Since the focal length of the parabola used is much larger than the few-micrometers Rayleigh length, the measured beam profiles correspond to the angular distribution of the generated harmonics and so can be used to determine their divergence [Fig. 4(a)]. At the plasma scale length of $L_p = 0.22\lambda$, close to efficiency optimum, the XUV beam profile has an almost Gaussian shape [Fig. 6(b)] corresponding to a quite low divergence [Fig. 4(a)]. For larger plasma scale lengths, the light-induced plasma surface deformation ("denting" [41]) becomes too strong, resulting in a destroyed beam profile [Fig. 6(d)] and a rapidly increasing divergence [Fig. 4(a)] as well as in a fuzzy harmonics spectral structure [Fig. 5(d)] [42]. Thus, the optimum plasma scale length is $L_p \approx 0.2\lambda$, which was used in the following experiment on the CEP dependence of harmonics.

The measured spectrum, energy, and divergence of the generated harmonics correspond to about 5×10^{28} and 2×10^{27} ph/(smm^2 mrad^2 1% bandwidth) at 30 eV and 70 eV, respectively, assuming the source diameter of 1 μm being equal to the focal spot size of the driving pulse (see Supplement 1 or [16]) and the pulse duration of 0.2 fs. Both assumptions are conservative and result in a slight underestimation of the maximum performance (the assumed pulse duration, e.g., is larger than the transform limit due to the necessary beamline dispersion control, including compensation of the filter dispersion). Nevertheless, this peak brilliance is not substantially worse compared to the XFEL performance in the XUV spectral range (Fig. 1).

4. CEP DEPENDENCE

The measured CEP dependence of the generated harmonics is shown in Fig. 7(a). Note that harmonics above 33 eV are generated by relativistic mechanisms [14,43], since the CWE process [37,44] can contribute only to the emission of photons with energy <33 eV determined by the maximum plasma frequency when ionizing a BK7 target. The corresponding result of a 1D PIC simulation [38] is presented in Fig. 7(b). Both figures show the following features: (I) a clear harmonic shift for positive CEP values by about one harmonic order; (II) the harmonic signal has a maximum at ~ -0.5 rad and drops to a minimum when the phase changes by about $\pi/2$, i.e., at $\sim +1$ rad and ~ -2 rad; and (III) around −2 rad, there is a subharmonic structure, namely, small additional peaks between main harmonics.

For comparison, the simulation results for slightly different plasma scale lengths are presented in Figs. 7(c)–7(d). The CEP dependence of the harmonic position shift and of the integrated harmonic yield for these results obviously differ both from the experimental data and the simulations for $L_p = 0.2\lambda$, which supports our estimation of the experimental plasma scale length of $L_p = 0.2\lambda$. Therefore, this approach can be used as a method to infer the plasma scale length from the CEP dependence of the relativistic surface high-order harmonics, which, although not direct and not single-shot as some other approaches [31,33], can be useful for providing information on the plasma scale length in similar experiments without additional experimental effort.

The agreement between experimental data and simulations for $L_p = 0.2\lambda$ is even more prominently visible in the single-shot spectra shown in Fig. 8, where the slow modulation in the harmonic spectral amplitude and the modulation depth of the harmonic peaks are in fair agreement. In addition, one can clearly see from both experimental data and simulations that the smallest spectral modulation depth [Fig. 8(a)] coincides with the best isolation degree (as will be discussed in the following), whereas modulation depth is considerably larger [Fig. 8(b)] for CEP values corresponding to a temporal structure with 2–3 pulses in the train. Furthermore, the measured spectra can be used for evaluation of both variation in the pulse spacing averaged over the train (ΔT) as CEP changes and the value of uneven spacing between pulses in the train (δT). The presence of the last effect is clear from the beating structure in the measured XUV spectra, which is most pronounced in the CEP $= \pi/2$ case [Fig. 8(b)] and

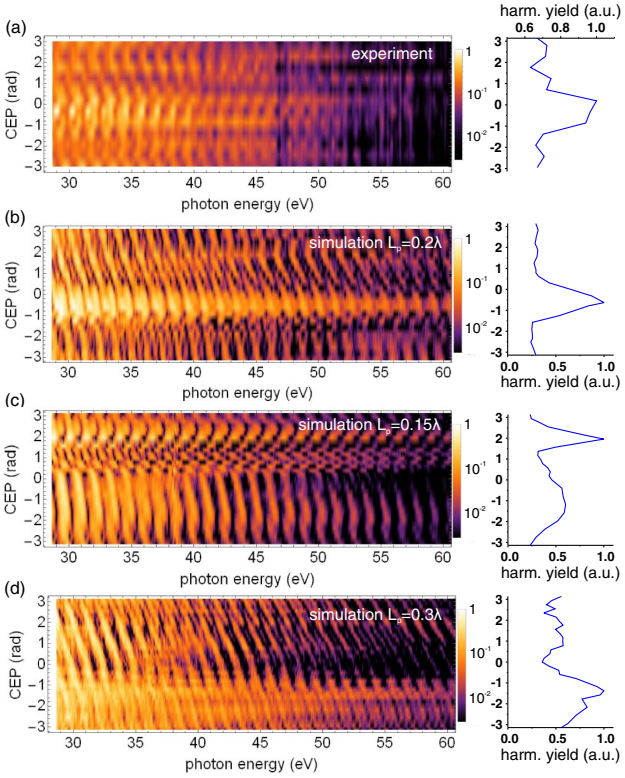

Fig. 7. Dependence of the harmonic spectrum (left panels) and the integrated harmonic yield (right panels) on the CEP of the driving field. (a) Measurements (consisting of shots acquired over 20 min and sorted according to their CEP values). (b)–(e) PIC simulations for different plasma scale lengths L_p (simulation parameters: $a_0 = 3$, $\tau = 2.5\lambda/c \sim 7$ fs, (b) $L_p = 0.2\lambda$, (c) $L_p = 0.15\lambda$, and (d) $L_p = 0.3\lambda$). CEP = 0 corresponds to a cosine waveform with the maximum of the carrier wave in synchrony with the intensity envelope.

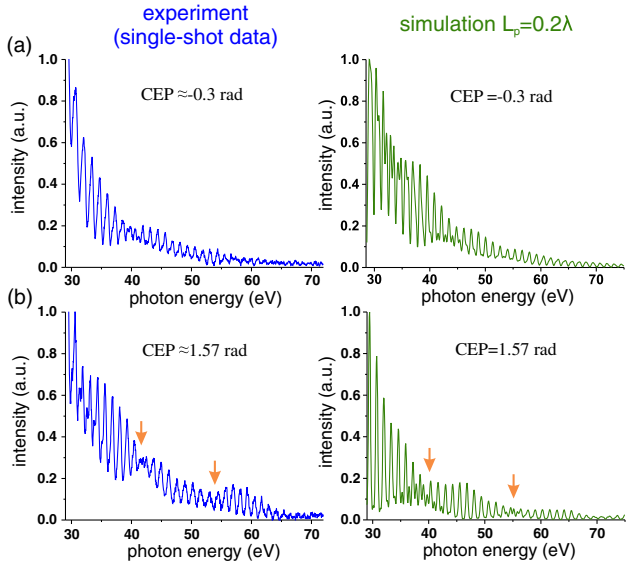

Fig. 8. XUV spectra for different CEP values: single-shot experimental results (left panels) and line-outs of simulation (right panels). (a) Case with the smallest modulation depth and best isolation degree [cf. Fig. 9(d) and the main text for details]. (b) Case with a pronounced beating structure (beating nodes are marked with arrows), which corresponds to the generation of three attosecond pulses with nearly equal amplitudes.

signifies that there are about three attosecond pulses with uneven temporal spacing [44].

The measured CEP dependence [Fig. 7(a)] shows that, e.g., for the $n = 25$-th harmonic (35 eV), the maximum deviation from its original position, when scanning the CEP from $-\pi$ to π, is about 1.4 eV, which is nearly one harmonic order. This corresponds to a change ΔT in the average pulse separation by $\Delta T = T_0/n = 120$as (see Supplement 1 for details), where $T_0 = 3$ fs is the period of the carrier. Nearly the same shift is observed in the simulations where the delay between attosecond pulses changes by 140 as [Fig. 9(b)].

The period of the beating structure in the measured spectrum [Fig. 8(b)] is $f_{\text{beating}} = 15 \pm 1.5$ eV, which corresponds to $\delta T = 1/f_{\text{beating}} = 270 \pm 27$ as the difference in the temporal spacing between attosecond pulses in the pulse train (see Supplement 1 for details). The last result allows an estimation of the plasma denting [41], namely, the shift of the point of reflection from the plasma mirror by $\delta T \times c/(2\cos(45°)) = 57 \pm 6$ nm (see Supplement 1 for details on the derivation) during one optical cycle at the peak of the driving field under our experimental conditions. Although the effect of denting is smaller than the typical target alignment uncertainty and instability on the μm scale (see Supplement 1 for details), it is not limited by these parameters, since the measurements (Fig. 8) are single-shot and the measured features are determined by the laser-plasma interaction time of about 7 fs, within which the bulk of the target can be assumed to be perfectly still.

Thus, a thorough analysis of the CEP harmonics spectra provides information on the plasma scale length and plasma dynamics during interaction. The temporal structure of the emitted XUV radiation is discussed in the following.

5. TEMPORAL STRUCTURE

Applying the spectral transmission corresponding to an aluminum (Al) filter (17–70 eV transmission window), the temporal structure of XUV radiation from the data set in Fig. 7(b) is shown in Fig. 9. From the energy ratio between the main attosecond pulse and the rest of the train, it is evident that within nearly one half of the CEP range, namely, between −2 rad and 0.5 rad, the XUV emission is confined mostly within one attosecond pulse. Using the intensity ratio between the main attosecond pulse and the rest of the train as the figure of merit for the degree of pulse isolation, the optimum CEP value under our experimental conditions is −0.3 rad. In this case, 74% of the overall energy of the pulse train is contained within a quasi-isolated attosecond pulse [orange line in Fig. 9(d)] that has a contrast of 0.16. The energy content and the contrast can be improved to 86% and 4×10^{-2}, respectively, using a bandpass XUV filter with a 10 eV bandwidth centered at 45 eV, which infers the generation of an isolated attosecond pulse [blue line in Fig. 9(d)]. These results provide strong evidence for the possibility to generate isolated attosecond pulses in the presented setup. However, additional experiments on the temporal characterization and application of these pulses should follow our work for the final proof of this scenario.

Theoretical discussions of the mechanisms supporting the generation of isolated attosecond pulses under conditions close to the ones in the performed experiments can be found

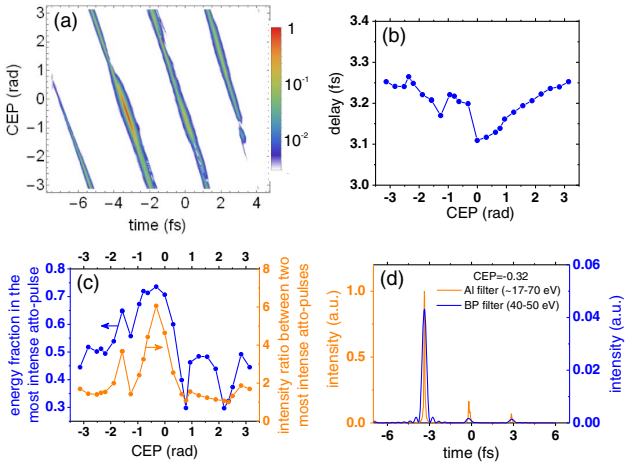

Fig. 9. Temporal structure of the attosecond trace for $L_p = 0.2\lambda$ from the PIC simulations. (a) CEP dependence of the temporal structure of the attosecond pulse train (transmission of an Al filter is applied). (b) Averaged delay (ΔT) between attosecond pulses. (c) Energy (blue-dotted line) and intensity (orange-dotted line) ratio between the main attosecond pulse and the rest of the train. (d) Quasi-isolated attosecond pulse for CEP = −0.32 rad, Al filter (orange line) and isolated attosecond pulse for the case of CEP = −0.32 rad, and bandpass (BP) filter with 10 eV bandwidth centered at 45 eV (blue line). In these simulations, $a_0 = 3$, $\tau = 2.5\lambda/c \sim 7$ fs, $L_p = 0.2\lambda$.

elsewhere [18,43,45,46]; however, for clarity, we shortly summarize the main ideas and put them into perspective with the obtained experimental results. The previous works [18,43,45,46] predict the importance of the plasma scale length optimization. Indeed, our simulations confirm that the CEP dependence and with it the temporal structure of the generated XUV pulses critically depend on the plasma scale length, which is exemplified in Fig. 7 and additionally by comparison of the data in Fig. 9 and an extra set of calculations in Supplement 1, where $L_p = 0.05\lambda$, i.e., a smaller scale length, was used with otherwise identical parameters. An analysis of the results of the PIC simulations for these two cases revealed clear differences in spectral and temporal structures (i.e., practically no CEP dependence of the generated spectrum and no isolated attosecond pulse at $L_p = 0.05\lambda$) as well as in the electron plasma density at the moment of the attosecond pulse generation shown in Fig. 10. While for $L_p = 0.2\lambda$, an electron bunch with about 5 nm layer thickness is created, no such feature is present for $L_p = 0.05\lambda$. This can be related

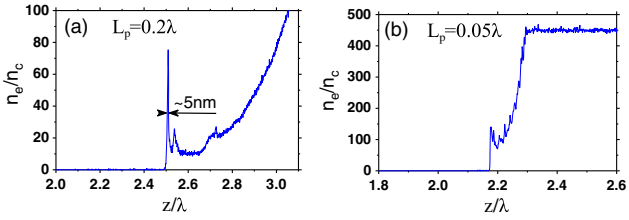

Fig. 10. Plasma electron density (n_e) right before the generation of the most intense attosecond pulse. Results of PIC simulations for $a_0 = 3$, $\tau = 2.5\lambda/c \sim 7$ fs, CEP = −0.32 rad, and: (a) $L_p = 0.2\lambda$ [corresponding temporal structure is presented in Fig. 9(d)]; (b) $L_p = 0.05\lambda$. n_c is the critical plasma density.

to the steeper density gradient in the latter case, where electrons at the plasma edge are just pushed into the bulk rather than bunched into a thin layer. A more detailed analysis of this effect can be found in [45]. The simulations also show that for $L_p = 0.2\lambda$, the position of the electron nano-bunch shifts deeper inside the plasma with every subsequent optical cycle. This already-mentioned effect of the so-called plasma denting [41] causes an increase in the temporal spacing between the pulses in the generated attosecond pulse train as well as dephasing between the incoming electric field and plasma motion. Since the magnitude of each shift is determined by the field strength of the previous optical cycle, which depends on the CEP, there is a dependence of the attosecond pulse spacing and thus the harmonic spectral structure on the CEP of the driving field. This dephasing and denting act as a gating mechanism that supports the generation of isolated attosecond pulses even with about 3 cycle IR pulses. Additional examples of PIC simulations, their description, and further technical details can be found in Supplement 1.

The possibility to generate isolated attosecond pulses with 2–3-cycle driving fields under optimized pre-plasma scale length and CEP is a very important result, because it infers that the relativistic surface high harmonics have not only higher conversion efficiency but also many fewer strict requirements on the duration of the driving field compared to gas harmonics, where nearly single cycle optical fields are necessary to generate isolated attosecond pulses. This makes the relativistic surface high harmonics a very promising source of isolated intense attosecond pulses.

6. CONCLUSION

By utilizing high-field few-cycle laser pulses, we have demonstrated the efficient generation of high-quality, intense relativistic high-order harmonics from solid surfaces at optimized pre-plasma parameters. The conditions supporting the generation of isolated attosecond XUV pulses are identified by measuring the dependence of the harmonics spectrum on the CEP of the driving field. Also, the possibility to estimate the plasma dynamics during laser–plasma interaction using the measured harmonics CEP dependence is presented. The demonstrated XUV pulse energy level of several μJ and the finding that already an ∼3 cycle driving field can produce an isolated attosecond pulse, in combination with the availability of CEP stable, high-intensity, high-repetition-rate, few-cycle laser pulses [16,17,47], commence a new era of experimental investigations in ultrafast nonlinear XUV optics [4,48] using relativistic surface high-order harmonics.

Funding. Max-Planck-Gesellschaft (MPG) (IMPRS-APS, PFS-grant); Deutsche Forschungsgemeinschaft (DFG) (EXC 158, TR-18); Horizon 2020 Framework Programme (H2020) (633053 within the framework of the EUROfusion); European Regional Development Fund (ERDF) (GINOP-2.3.6-15-2015-00001).

Acknowledgment. The authors acknowledge the contribution of former members of the team: I. Ahmad, S. Klingebiel, C. Wandt, A. Schwarz, and C. Skrobol. Furthermore, we thank M. Schultze, A. Guggenmos, B. Bergues, E. Goulielmakis, M. Ossiander, F. Siegrist, U. Kleineberg, M. Weidman,

T. T. Luu, Q. Liu, M. Kling, M. Gilljohann, V. Yakovlev, and M. Ciappina for helpful discussions.

See Supplement 1 for supporting content and Visualization 1 for animated representation of the laser–plasma interaction. Comprehensive comments to Visualization 1 are given in Chapter 4 of Supplement 1.

REFERENCES

1. A. L'Huillier and P. Balcou, "High-order harmonic generation in rare gases with a 1-ps 1053-nm laser," Phys. Rev. Lett. **70**, 774–777 (1993).
2. M. Hentschel, R. Kienberger, C. Spielmann, G. A. Reider, N. Milosevic, T. Brabec, P. Corkum, U. Heinzmann, M. Drescher, and F. Krausz, "Attosecond metrology," Nature **414**, 509–513 (2001).
3. P. M. Paul, E. S. Toma, P. Breger, G. Mullot, F. Augé, P. Balcou, H. G. Muller, and P. Agostini, "Observation of a train of attosecond pulses from high harmonic generation," Science **292**, 1689–1692 (2001).
4. F. Krausz and M. Ivanov, "Attosecond physics," Rev. Mod. Phys. **81**, 163–234 (2009).
5. F. Krausz and M. I. Stockman, "Attosecond metrology: from electron capture to future signal processing," Nat. Photonics **8**, 205–213 (2014).
6. M. Reduzzi, P. Carpeggiani, S. Kühn, F. Calegari, M. Nisoli, S. Stagira, C. Vozzi, P. Dombi, S. Kahaly, P. Tzallas, D. Charalambidis, K. Varju, K. Osvay, and G. Sansone, "Advances in high-order harmonic generation sources for time-resolved investigations," J. Electron Spectrosc. Relat. Phenom. **204**, 257–268 (2015).
7. E. J. Takahashi, P. Lan, O. D. Mücke, Y. Nabekawa, and K. Midorikawa, "Attosecond nonlinear optics using gigawatt-scale isolated attosecond pulses," Nat. Commun. **4**, 2691 (2013).
8. A. Nayak, I. Orfanos, I. Makos, M. Dumergue, S. Kühn, E. Skantzakis, B. Bodi, K. Varju, C. Kalpouzos, H. I. B. Banks, A. Emmanouilidou, D. Charalambidis, and P. Tzallas, "Multiple ionization of argon via multi-XUV-photon absorption induced by 20-GW high-order harmonic laser pulses," Phys. Rev. A **98**, 023426 (2018).
9. B. Bergues, D. E. Rivas, M. Weidman, A. A. Muschet, W. Helml, A. Guggenmos, V. Pervak, U. Kleineberg, G. Marcus, R. Kienberger, D. Charalambidis, P. Tzallas, H. Schröder, F. Krausz, and L. Veisz, "Tabletop nonlinear optics in the 100-eV spectral region," Optica **5**, 237–242 (2018).
10. D. Popmintchev, B. R. Galloway, M.-C. Chen, F. Dollar, C. A. Mancuso, A. Hankla, L. Miaja-Avila, G. O'Neil, J. M. Shaw, G. Fan, S. Ališauskas, G. Andriukaitis, T. Balčiunas, O. D. Mücke, A. Pugzlys, A. Baltuška, H. C. Kapteyn, T. Popmintchev, and M. M. Murnane, "Near- and extended-edge x-ray-absorption fine-structure spectroscopy using ultrafast coherent high-order harmonic supercontinua," Phys. Rev. Lett. **120**, 093002 (2018).
11. T. Popmintchev, M.-C. Chen, D. Popmintchev, P. Arpin, S. Brown, S. Ališauskas, G. Andriukaitis, T. Balčiunas, O. D. Mücke, A. Pugzlys, A. Baltuška, B. Shim, S. E. Schrauth, A. Gaeta, C. Hernández-García, L. Plaja, A. Becker, A. Jaron-Becker, M. M. Murnane, and H. C. Kapteyn, "Bright coherent ultrahigh harmonics in the keV x-ray regime from mid-infrared femtosecond lasers," Science **336**, 1287–1291 (2012).
12. L. Plaja, L. Roso, K. Rzażewski, and M. Lewenstein, "Generation of attosecond pulse trains during the reflection of a very intense laser on a solid surface," J. Opt. Soc. Am. B **15**, 1904–1911 (1998).
13. G. D. Tsakiris, K. Eidmann, J. M. ter Vehn, and F. Krausz, "Route to intense single attosecond pulses," New J. Phys. **8**, 19 (2006).
14. T. Baeva, S. Gordienko, and A. Pukhov, "Theory of high-order harmonic generation in relativistic laser interaction with overdense plasma," Phys. Rev. E **74**, 046404 (2006).
15. P. Heissler, R. Hörlein, J. M. Mikhailova, L. Waldecker, P. Tzallas, A. Buck, K. Schmid, C. M. S. Sears, F. Krausz, L. Veisz, M. Zepf, and G. D. Tsakiris, "Few-cycle driven relativistically oscillating plasma mirrors: a source of intense isolated attosecond pulses," Phys. Rev. Lett. **108**, 235003 (2012).
16. A. Kessel, V. E. Leshchenko, O. Jahn, M. Krüger, A. Münzer, A. Schwarz, V. Pervak, M. Trubetskov, S. A. Trushin, F. Krausz, Z. Major, and S. Karsch, "Relativistic few-cycle pulses with high contrast from picosecond-pumped OPCPA," Optica **5**, 434–442 (2018).
17. D. E. Rivas, A. Borot, D. E. Cardenas, G. Marcus, X. Gu, D. Herrmann, J. Xu, J. Tan, D. Kormin, G. Ma, W. Dallari, G. D. Tsakiris, I. B. Földes, S. W. Chou, M. Weidman, B. Bergues, T. Wittmann, H. Schröder, P. Tzallas, D. Charalambidis, O. Razskazovskaya, V. Pervak, F. Krausz, and L. Veisz, "Next generation driver for attosecond and laser-plasma physics," Sci. Rep. **7**, 5224 (2017).
18. G. Ma, W. Dallari, A. Borot, F. Krausz, W. Yu, G. D. Tsakiris, and L. Veisz, "Intense isolated attosecond pulse generation from relativistic laser plasmas using few-cycle laser pulses," Phys. Plasmas **22**, 033105 (2015).
19. S. Corde, K. Ta Phuoc, G. Lambert, R. Fitour, V. Malka, A. Rousse, A. Beck, and E. Lefebvre, "Femtosecond x rays from laser-plasma accelerators," Rev. Mod. Phys. **85**, 1–48 (2013).
20. A. Döpp, L. Hehn, J. Götzfried, J. Wenz, M. Gilljohann, H. Ding, S. Schindler, F. Pfeiffer, and S. Karsch, "Quick x-ray microtomography using a laser-driven betatron source," Optica **5**, 199–203 (2018).
21. D. Kormin, A. Borot, G. Ma, W. Dallari, B. Bergues, M. Aladi, I. B. Földes, and L. Veisz, "Spectral interferometry with waveform-dependent relativistic high-order harmonics from plasma surfaces," Nat. Commun. **9**, 4992 (2018).
22. C. Rödel, D. an der Brügge, J. Bierbach, M. Yeung, T. Hahn, B. Dromey, S. Herzer, S. Fuchs, A. G. Pour, E. Eckner, M. Behmke, M. Cerchez, O. Jäckel, D. Hemmers, T. Toncian, M. C. Kaluza, A. Belyanin, G. Pretzler, O. Willi, A. Pukhov, M. Zepf, and G. G. Paulus, "Harmonic generation from relativistic plasma surfaces in ultrasteep plasma density gradients," Phys. Rev. Lett. **109**, 125002 (2012).
23. B. Dromey, M. Zepf, A. Gopal, K. Lancaster, M. S. Wei, K. Krushelnick, M. Tatarakis, N. Vakakis, S. Moustaizis, R. Kodama, M. Tampo, C. Stoeckl, R. Clarke, H. Habara, D. Neely, S. Karsch, and P. Norreys, "High harmonic generation in the relativistic limit," Nat. Phys. **2**, 456–459 (2006).
24. B. Dromey, S. Kar, C. Bellei, D. C. Carroll, R. J. Clarke, J. S. Green, S. Kneip, K. Markey, S. R. Nagel, P. T. Simpson, L. Willingale, P. McKenna, D. Neely, Z. Najmudin, K. Krushelnick, P. A. Norreys, and M. Zepf, "Bright multi-keV harmonic generation from relativistically oscillating plasma surfaces," Phys. Rev. Lett. **99**, 085001 (2007).
25. European XFEL, https://www.xfel.eu.
26. SLAC, https://heds.slac.stanford.edu/our-research/record-peak-brightness.
27. S. H. Glenzer, L. B. Fletcher, E. Galtier, B. Nagler, R. Alonso-Mori, B. Barbrel, S. B. Brown, D. A. Chapman, Z. Chen, C. B. Curry, F. Fiuza, E. Gamboa, M. Gauthier, D. O. Gericke, A. Gleason, S. Goede, E. Granados, P. Heimann, J. Kim, D. Kraus, M. J. MacDonald, A. J. Mackinnon, R. Mishra, A. Ravasio, C. Roedel, P. Sperling, W. Schumaker, Y. Y. Tsui, J. Vorberger, U. Zastrau, A. Fry, W. E. White, J. B. Hasting, and H. J. Lee, "Matter under extreme conditions experiments at the Linac Coherent Light Source," J. Phys. B **49**, 092001 (2016).
28. N. R. Council, *Controlling the Quantum World: The Science of Atoms, Molecules, and Photons* (The National Academies, 2007).
29. C. Bostedt, S. Boutet, D. M. Fritz, Z. Huang, H. J. Lee, H. T. Lemke, A. Robert, W. F. Schlotter, J. J. Turner, and G. J. Williams, "Linac coherent light source: the first five years," Rev. Mod. Phys. **88**, 015007 (2016).
30. W. Helml, A. R. Maier, W. Schweinberger, I. Grguras, P. Radcliffe, G. Doumy, C. Roedig, J. Gagnon, M. Messerschmidt, S. Schorb, C. Bostedt, F. Grüner, L. F. DiMauro, D. Cubaynes, J. D. Bozek, T. Tschentscher, J. T. Costello, M. Meyer, R. Coffee, S. Düsterer, A. L. Cavalieri, and R. Kienberger, "Measuring the temporal structure of few-femtosecond free-electron laser x-ray pulses directly in the time domain," Nat. Photonics **8**, 950–957 (2014).
31. S. Kahaly, S. Monchocé, H. Vincenti, T. Dzelzainis, B. Dromey, M. Zepf, P. Martin, and F. Quéré, "Direct observation of density-gradient effects in harmonic generation from plasma mirrors," Phys. Rev. Lett. **110**, 175001 (2013).
32. F. Dollar, P. Cummings, V. Chvykov, L. Willingale, M. Vargas, V. Yanovsky, C. Zulick, A. Maksimchuk, A. G. R. Thomas, and K. Krushelnick, "Scaling high-order harmonic generation from laser-solid interactions to ultrahigh intensity," Phys. Rev. Lett. **110**, 175002 (2013).
33. K. Adumi, K. A. Tanaka, T. Matsuoka, T. Kurahashi, T. Yabuuchi, Y. Kitagawa, R. Kodama, K. Sawai, K. Suzuki, K. Okabe, T. Sera, T. Norimatsu, and Y. Izawa, "Characterization of preplasma produced by an ultrahigh intensity laser system," Phys. Plasmas **11**, 3721–3725 (2004).

34. J. E. Crow, P. L. Auer, and J. E. Allen, "The expansion of a plasma into a vacuum," J. Plasma Phys. **14**, 65–76 (1975).
35. A. Baltuska, M. Uiberacker, E. Goulielmakis, R. Kienberger, V. S. Yakovlev, T. Udem, T. W. Hansch, and F. Krausz, "Phase-controlled amplification of few-cycle laser pulses," IEEE J. Sel. Top. Quantum Electron. **9**, 972–989 (2003).
36. C. Li, E. Moon, H. Wang, H. Mashiko, C. M. Nakamura, J. Tackett, and Z. Chang, "Determining the phase-energy coupling coefficient in carrier-envelope phase measurements," Opt. Lett. **32**, 796–798 (2007).
37. F. Quéré, C. Thaury, P. Monot, S. Dobosz, P. Martin, J.-P. Geindre, and P. Audebert, "Coherent wake emission of high-order harmonics from overdense plasmas," Phys. Rev. Lett. **96**, 125004 (2006).
38. R. Lichters, J. Meyer-ter Vehn, and A. Pukhov, "Short-pulse laser harmonics from oscillating plasma surfaces driven at relativistic intensity," Phys. Plasmas **3**, 3425–3437 (1996).
39. P. Heissler, A. Barna, J. M. Mikhailova, G. Ma, K. Khrennikov, S. Karsch, L. Veisz, I. B. Földes, and G. D. Tsakiris, "Multi-μJ harmonic emission energy from laser-driven plasma," Appl. Phys. B **118**, 195–201 (2015).
40. G. Sansone, L. Poletto, and M. Nisoli, "High-energy attosecond light sources," Nat. Photonics **5**, 655–663 (2011).
41. H. Vincenti, S. Monchocé, S. Kahaly, G. Bonnaud, P. Martin, and F. Quéré, "Optical properties of relativistic plasma mirrors," Nat. Commun. **5**, 3403 (2013).
42. M. Behmke, D. an der Brügge, C. Rödel, M. Cerchez, D. Hemmers, M. Heyer, O. Jäckel, M. Kübel, G. G. Paulus, G. Pretzler, A. Pukhov, M. Toncian, T. Toncian, and O. Willi, "Controlling the spacing of attosecond pulse trains from relativistic surface plasmas," Phys. Rev. Lett. **106**, 185002 (2011).
43. D. an der Brügge and A. Pukhov, "Enhanced relativistic harmonics by electron nanobunching," Phys. Plasmas **17**, 033110 (2010).
44. A. Borot, A. Malvache, X. Chen, A. Jullien, J.-P. Geindre, P. Audebert, G. Mourou, F. Quéré, and R. Lopez-Martens, "Attosecond control of collective electron motion in plasmas," Nat. Phys. **8**, 416–421 (2012).
45. A. Gonoskov, "Theory of relativistic radiation reflection from plasmas," Phys. Plasmas **25**, 013108 (2018).
46. A. A. Gonoskov, A. V. Korzhimanov, A. V. Kim, M. Marklund, and A. M. Sergeev, "Ultrarelativistic nanoplasmonics as a route towards extreme-intensity attosecond pulses," Phys. Rev. E **84**, 046403 (2011).
47. R. Budriūnas, T. Stanislauskas, J. Adamonis, A. Aleknavičius, G. Veitas, D. Gadonas, S. Balickas, A. Michailovas, and A. Varanavičius, "53 W average power CEP-stabilized OPCPA system delivering 5.5 TW few cycle pulses at 1 kHz repetition rate," Opt. Express **25**, 5797–5806 (2017).
48. P. Tzallas, D. Charalambidis, N. A. Papadogiannis, K. Witte, and G. D. Tsakiris, "Direct observation of attosecond light bunching," Nature **426**, 267–271 (2003).